Archaeometry **53**, 2 (2011) 340–363 doi: 10.1111/j.1475-4754.2010.00545.x

IBERIAN CERAMIC PRODUCTION FROM BASTI (BAZA, SPAIN): FIRST GEOCHEMICAL, MINERALOGICAL AND TEXTURAL CHARACTERIZATION*

G. CULTRONE,[1] E. MOLINA,[1] C. GRIFA[2] and E. SEBASTIÁN[1]

[1]*Departamento Mineralogía y Petrología, Universdad de Granada, Avda. Fuentenueva s/n., 18002 Granada, Spain*
[2]*Dipartimento Studi Geologici ed Ambientali, Università del Sannio, Via dei Mulini 59/A, 82100 Benevento, Italy*

Ceramic fragments from the archaeological excavation of the Iberian–Roman city of Basti (Spain) were studied from a geochemical point of view and by applying a statistical tool to X-ray fluorescence data to discover similarities between ceramic materials. The analysis of these samples was completed by performing a mineralogical analysis, textural observation, and by characterizing the porous system and the colour of the pieces. Our results enabled us to identify the source area of the clayey raw material in the surroundings of Basti and to estimate the firing temperature of the ceramics. Differences in the chemistry were confirmed by characteristics of the pastes and the mineralogical composition of the pieces. Some samples show black cores, which would suggest the presence of organic matter in the raw material and fast firing of the ceramics. The main types of temper were quartz grains and gneiss fragments, although carbonate grains were also identified. Our evidence suggests that most of the samples were well fired. New silicate phases were found to be present in several samples. The mercury intrusion porosimetry verified and confirmed the firing temperature of non-carbonated samples. Colorimetry showed that the colour of the ceramics varied according to the amount of CaO that they contained.

KEYWORDS: IBERIAN CERAMIC, BASTI, GEOCHEMISTRY, FIRING TEMPERATURE, RAW MATERIAL PROVENANCE

INTRODUCTION

The archaeological site of Basti, an important Iberian–Roman city, is located on Cerro Cepero, a hill near the modern town of Baza (Granada, Spain; Fig. 1). This site includes the city itself, several necropoleis and various other structures (Adroher Auroux 2008). The beginnings of this settlement would seem to date back to the Copper Age, and there is direct evidence from the ninth century BC, a period of growth due to its strategic position on trade routes between the Mediterranean coast, the Phoenician ports and the inland Iberian peninsula. The Iberian and Roman occupations provided the greatest economic and technological inputs to the city. The city's growing influence reached its height in the fourth century BC. A city wall and one of the most important necropoleis in the area were built during this period. The discovery of the 'Dama de Baza', which had one of the most complete funeral dowries and became the most important surviving Iberian sculpture, shows the control exerted by these people over the area's resources (Gil Julià 2008). After the Roman conquest, the influence of the city remained strong as the route of the Via Herculea passed near this '*oppidum*', so highlighting its importance for trade in the Roman Empire.

*Received 20 April 2009; accepted 19 April 2010

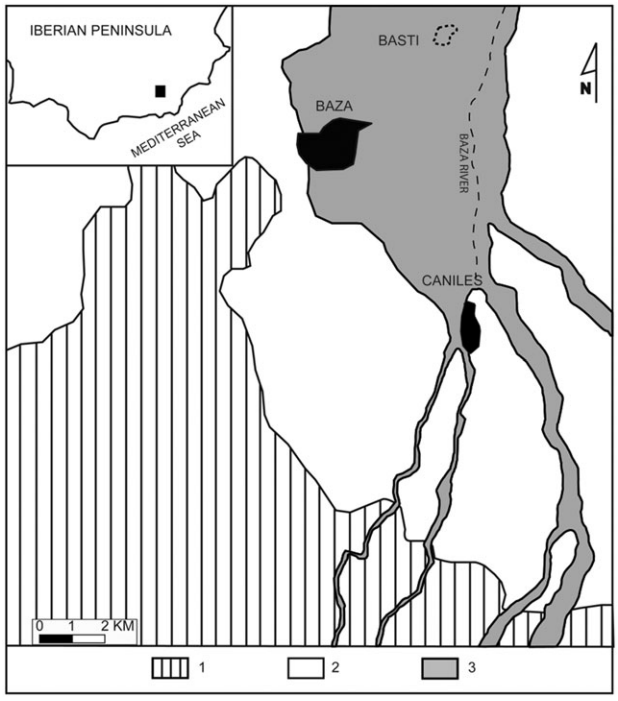

Figure 1 *The geological location of Basti (dashed line) near Baza (Andalusia, Spain): 1, the Alpujarride and Nevado Filabride Complexes; 2, Plio-Quaternary materials; 3, Quaternary fluvial materials.*

A number of different ceramic fragments have been uncovered in recent excavations at Cerro Cepero. Our work focused on the study of these materials, most of which date from the Iberian period. The types and ages of the fragments are set out in Table 1. Although little or no research has been done on ceramic production in Basti, there are several papers on this topic in other areas of the Iberian peninsula, such as the archaeometric studies on the composition and provenance of Phoenician and Iberian ceramics in the south of Spain, in the present-day provinces of Malaga (Cardell *et al*. 1999) and Seville (González Vílchez *et al*. 1985). Petit Domínguez *et al*. (2003) demonstrated how Iberian potters learned to prevent 'lime blowing' in amphorae manufacture when using clays rich in $CaCO_3$, by firing them at low temperatures (below 700°C). Some data have been provided about Iberian ceramic production in different parts of the north-east region of the Iberian peninsula and the trade in ceramics with neighbouring areas and peoples (Fernandes *et al*. 1998; Tsantini *et al*. 2005). Tsantini (2007) proposed hypotheses about the relationships between different Iberian peoples based on the production of amphorae using local clays and the trade with other areas. By estimating the firing temperature of the samples, the same author demonstrated that the majority of amphorae were well fired, which showed that the potters had achieved a relatively high level of technological development. Research at other sites showed a standardization in the selection of raw materials, their mixing, processing, decoration and the choice of firing conditions from the end of the fourth century BC onwards (Ordiozola and Hurtado Pérez 2007; Igea Romera *et al*. 2008).

Our aim was to carry out the first exhaustive characterization of the ceramics found at the Basti site, as so far they have not been the subject of scientific research. Ceramics provide an artistic

Table 1 *A list of the studied samples and some archaeological data. The analytical techniques performed on the samples are indicated as follows: XRF, X-ray fluorescence + statistical study; XRD, X-ray diffraction; POM, polarized optical microscopy; FESEM, field emission scanning electron microscopy; MIP, mercury intrusion porosimetry; C, colorimetry*

Sample	*Ceramic type*	*Age (centuries)*	*Techniques*
IB1	Small Visigoth wheel	5th–8th AD	XRF, XRD, POM, FESEM, C
IB2	Small Visigoth wheel	5th–8th AD	XRF, XRD, POM, FESEM, C
IB3	Iberian dish	7th–6th BC	XRF, XRD, POM, FESEM, MIP, C
IB4	Iberian dish	7th–6th BC	XRF, XRD, POM, FESEM, MIP, C
IB5	Iberian dish	7th–6th BC	XRF, XRD, POM, FESEM, MIP, C
IB6	Small urn	5th–1st BC	XRF, XRD, POM, FESEM, MIP, C
IB7	Iberian amphora	3rd–1st BC	XRF, XRD, POM, FESEM, MIP, C
IB8	Iberian amphora (handle)	6th–5th BC	XRF, XRD, POM, FESEM, MIP, C
IB9	Phoenician or Iberian amphora	8th–7th BC	XRF, XRD, POM, FESEM, MIP, C
IB10	Unknown	2nd–1st BC	XRF, XRD, MIP, C
IB11	Iberian amphora	4th BC	XRF, XRD, MIP, C
IB12	Iberian amphora	7th–6th BC	XRF, XRD, POM, FESEM, MIP, C
IB13	Iberian amphora	6th–5th BC	XRF, XRD, POM, FESEM, MIP, C
IB14	Iberian amphora (handle)	7th–5th BC	XRF, XRD, POM, FESEM, MIP, C
IB15	Iberian amphora	5th–3rd BC	XRF, XRD, POM, FESEM, MIP, C
IB16	Iberian amphora	2nd–1st BC	XRF, XRD, POM, FESEM, MIP, C
IB17	Iberian amphora	2nd–1st BC	XRF, XRD, MIP, C
IB18	Iberian amphora	3rd?–1st BC	XRF, XRD, MIP, C
IB19	Phoenician or Iberian amphora	8th–7th BC	XRF, XRD, POM, FESEM, MIP, C
IB20	Iberian amphora	6th–5th BC	XRF, XRD, POM, FESEM, MIP, C
IB21	Iberian amphora	4th–3rd BC	XRF, XRD, POM, FESEM, MIP, C
IB22	Iberian amphora	2nd BC	XRF, XRD, MIP, C
IB23	Iberian amphora	3rd–2nd BC	XRF, XRD, POM, FESEM, MIP, C
IB24	Iberian amphora	6th–5th BC	XRF, XRD, POM, FESEM, C
IB25	Iberian amphora	4th–2nd BC	XRF, XRD, MIP, C
IB26	Iberian amphora	8th?–6th BC	XRF, XRD, POM, FESEM, C
IB27	Iberian amphora	4th–2nd BC	XRF, XRD, MIP, C
IB28	Iberian amphora	2nd BC–1st AD	XRF, XRD, POM, FESEM, MIP, C
IB29	Iberian amphora	4th BC	XRF, XRD, POM, FESEM, MIP, C
IB30	Iberian amphora	3rd–2nd BC	XRF, XRD, MIP, C
IB31	Iberian amphora	3rd–2nd BC	XRF, XRD, POM, FESEM, MIP, C
IB32	Iberian amphora	3rd–1st BC	XRF, XRD, POM, FESEM, MIP, C
IB33	Iberian amphora	5th–4th BC	XRF, XRD, POM, FESEM, MIP, C
IB34	Phoenician or Iberian amphora	8th–7th BC	XRF, XRD, MIP, C
IB35	Iberian amphora	5th–4th BC	XRF, XRD, MIP, C

and technological insight into the people who produced them, and as we have no other data to work with, these are our only source of information about the production area and about the local economy and society. In applying different analytical techniques, our aim was to try to discover whether ceramic production had undergone any changes over the nine centuries of the period that we were studying (from the eighth century BC to the first century AD) in terms of the use of different raw materials and/or due to the specialization of the town of Basti in the making of ceramics. With this in mind, special attention was given to the textural and mineralogical composition of the ceramic pieces, and hypotheses were proposed as to the possible use of different raw materials and the choice of firing temperatures in the production process.

THE GEOLOGY OF THE AREA UNDER EXAMINATION

Cerro Cepero is located in the intra-mountain basin of Guadix–Baza, which developed during the Alpine folding of the Baetic Cordilleras. This basin developed from stages with marine deposits (Late Miocene) until it became silted up with a continental filling during the Pliocene and the Quaternary (Viseras *et al*. 2004). This basin has two clear depocentres and has therefore traditionally been divided into two sub-basins: the Guadix sub-basin and the Baza sub-basin. The Guadix sub-basin is situated in the western part, and is dominated by siliciclastic deposits from fluvial and alluvial environments with a highly varied grain size, which originate from the erosion of materials from the Internal Zones situated in the southern area and materials from the Sub-Betic/Pre-Betic sedimentary cover located in the northern area (Fernández *et al*. 1996; Soria and Viseras 2008). The Baza sub-basin lies in the eastern part, which is characterized by a filling of lacustrine materials in which limestone strata and layers of gypsum alternate with marly strata (Gibert *et al*. 2007). It is also interspersed, however, with levels with a higher proportion of terrigenous sediments, which have the same origin as the Guadix sub-basin. The fact that the marly gypsum-based materials erode easily compared to the relative hardness of the more carbonated strata led to the development of very soft hillocky shapes through which small streams flow (Pérez Peña *et al*. 2009).

The city of Basti is situated in the Baza sub-basin, and was built on top of the most recent deposits that contain lacustrine filling, and other deposits produced by the erosion of the main river that drains this sub-basin, the River Baza. It is important to point out that the sediments transported by this river are metamorphic materials from the Palaeozoic and the Permo-Triassic and are composed mainly of phyllites, schists, gneisses, quartzites, marbles and dolomites (Vera *et al*. 2004).

MATERIALS AND METHODS

Description of the samples

We studied a total of 35 ceramic fragments (Table 1), 28 of which belonged to Iberian amphorae from the period running from the eighth century BC to the first century AD. There were also three Iberian dishes made with a grey paste (seventh to sixth century BC), a small urn with a pronounced neck (fifth to first century BC), two Visigoth potter's wheels (fifth to eighth century AD) and another fragment of undetermined nature (second to first century BC). All of these came from the settlement at Basti, except for two of the three Iberian dishes (samples IB3 and IB4), which came from two small sites near Basti (Barranco Morenate and Cortijo de Bastida, respectively). These are so far the only samples uncovered by archaeological excavation in the area. Because of their particular shape, three of the amphora fragments (samples IB9, IB19 and IB34) are thought to be of Phoenician origin and to have come from the coast of Almeria, even though they were found at the Basti archaeological site.

At a macroscopic level, all the materials are a red-to-yellow colour except for the potter's wheel IB1, which has a colour scale that varies from black to red from the outside to the inside. Six other samples, which are reddish on the outside (IB8, IB9, IB14, IB26, IB29 and IB34), when cut perpendicular to the surface present what is known as a 'black core' or a dark-coloured core. In the literature, these cores are considered to have been formed as a result of three main factors; namely, the presence of reducing substances in the raw material (i.e., organic matter—Cardell *et al*. 1999; Maritan 2004; Pavía 2006), the use of high-plasticity clays that give the ceramic paste

a fine porosity, and fast firing (Cerdeño del Castillo *et al*. 2000; Buxeda i Garrigós *et al*. 2003; Tsantini 2007). These factors hindered diffusion of oxygen to the inside of the ceramic body, thus creating the conditions for reduction (and the dark colours) (Veniale 1990; Ricciardi *et al*. 2008).

Analytical techniques

Bulk chemical quantitative analyses were performed by means of X-ray fluorescence (XRF; S4 Pioneer, Bruker AXS). Samples weighing 5 g were finely ground and well mixed in an agate mortar before being pressed into an Al holder for disc preparation. ZAF correction was performed systematically (Scott and Love 1983). NCS DC 74301 (GSMS-1) standard (Chen and Wang 1998) was applied. Ten major and minor elements and nine trace elements were measured. The major and minor element contents are reported as wt% oxide normalized to 100%, while trace elements are expressed in ppm, LOI-free. The estimated accuracy for major elements is below 6%, except for K (8%), while that for trace elements is below 2%, except for Sr (7.5%). The precision was lower than 1%, except for Mn and Rb elements, which present values ranging from 1.35 to 1.62% (Niembro Bueno 2009).

If we assume that ceramics prepared with the same raw material have a similar chemical make-up, then differences in chemical composition can be interpreted as changes in the supply of local clays (Hein *et al*. 2004). With this in mind, we performed a statistical study based on the data obtained by XRF and grouped together the materials on the basis of chemically similar concentrations. Statistical multivariate analysis was performed using R software for Mac 2.4.1 (R Development Team 2005). First, the chemical data were $\log_{10}$-transformed to avoid the risk of misleading classification of the objects and to standardize all the components by giving them all the same 'weight' (Baxter 2001; Aruga 2003; Hall 2004). The initial data set was reduced for some of the major, minor and trace elements, such as Mn, P and Ba, since the concentration of these elements may be influenced by post-depositional phenomena due to the fact that the pieces have been buried for centuries (Maggetti *et al*. 1988; Fabbri *et al*. 1994; Maggetti 2001; García Heras *et al*. 2006). Other elements that showed low quantities, such as Nb and Y, were also excluded because they could distort the calculation with background noise (Grifa *et al*. 2009). Maggetti (2001) suggested that the Ca content should also be excluded from the calculation, because its concentration could be altered by water circulation in the soil that can deposit carbonates on the surface or in the pores of the shards. On the other hand, the Ca value can provide significant information about the raw materials used in the manufacture of ceramics and can provide clues about technological aspects of ceramic production; Ca is, in fact, one of the main elements that regulate the pyrometamorphic reaction during firing processes (Cultrone *et al*. 2001). We therefore decided to consider CaO in the statistical procedures, taking care to estimate the post-depositional alteration of chemical variables by other parameters such as P_2O_5 and LOI values (Fabbri *et al*. 1994).

We then carried out principal component (PCA) and hierarchical clustering analyses (HCA) on a reduced data set to achieve our geochemical and statistical objectives. Once chemical groups were established, polarized optical microscopy was used to find differences in the mineralogy, morphology and distribution of temper, and the degree of vitrification of the matrix samples. We used an Olympus BX-60 microscope coupled with a digital microphotography unit (Olympus DP-10).

The analysis of microtexture, the detection of primary and secondary porosity and the composition of small-sized mineral phases were further observed by means of a field emission scanning electron microscope (FESEM: Leo Gemini 1530) coupled with EDS microanalysis

(Oxford Inca 200). FESEM back-scattered electron (BSE) images were collected using polished thin carbon-coated sections.

X-ray diffraction (XRD) was used to define the mineralogical composition of the ceramics and to find out more about their firing temperature. A Philips PW 1710 diffractometer equipped with an automatic slit was used. The following conditions were applied: Cu–K_α radiation, 40 kV, 40 mA, 3° to 60° 2θ explored area and 0.1° 2θ s^{-1} goniometer speed. The diffractograms were interpreted using the XPowder software package (Martín 2004).

A Micromeritics AutoPore III 9410 mercury intrusion porosimeter (MIP) was used to measure the pore access size distribution and the open porosity of the samples, and to investigate whether or not these parameters are influenced by the type, composition and firing temperature of the ceramics. Freshly cut sample chips of ~2 cm^3 were oven dried for 24 h at 110°C and then analysed. Two MIP measurements were made per sample.

Colorimetry stands out among the techniques used to determine the physical properties of ceramics, because of its non-destructive nature. Colour measurement has already been used to characterize new (Stepkowska and Jefferis 1992; Nava and Riccardi 1999) and ancient ceramics (Molera *et al*. 1998; Mirti and Davit 2004). A portable Minolta CM700d spectrophotometer was used to determine the chromatic coordinates of ceramic fragments and to detect possible differences between samples because of their composition or production process. Due to the small size and curved surface of some samples, an illuminated area of just 3 mm in diameter was used. A pulsed xenon lamp with UV cut filter provided the illumination for the surface of the samples. A silicon photodiode array detected and measured both incident and reflected light. The measurements were performed by selecting CIE illuminant D65, which simulates daylight with a temperature colour of 6504 K.

The analytical techniques performed on each sample are indicated in Table 1.

RESULTS AND DISCUSSION

X-ray fluorescence and statistical study

The samples studied are rich in SiO_2 (values range between 46.9 and 63 wt%) and Al_2O_3 (15–24.2 wt%), presenting variable quantities of MgO, Fe_2O_3 and K_2O (Table 2). CaO content is also variable. In particular, as shown in Figure 2 (a), ceramic samples are divided into a small group characterized by low CaO content (less than 5–6 wt%) and a larger one with higher CaO values (more than 5–6 wt%), reaching in some cases up to 19 wt% (IB16, IB17 and IB18). The differences in CaO could be attributed to different compositions of raw material deliberately chosen by the potters depending on the particular purpose of the pieces they were going to make (e.g., cooking pots or food ware; Grifa *et al*. 2009) and/or to the addition of a carbonatic temper (Di Martino *et al*. 2005; Fabbri and Gualtieri 2007). In both cases this suggests that the potters had previous knowledge of how carbonates could contribute to the firing of ceramics. The existence of two main groups is confirmed by the comparison of other minor and trace elements, with some scattered samples lying outside these two groups (Figs 2 (b), 2 (c) and 2 (d)).

In order to compare the chemical variables in the XRF data set (Table 2) simultaneously, a multivariate statistical procedure was carried out. Principal component analysis (PCA) was used for the first step of the statistical calculation. By evaluating the cumulative proportion (Table 3), we showed that the statistical problem can be explained at the 11th Component (0.786; approximately 80% of the representativeness of the components selected from the whole variables), and

Table 2 *Selected major (in %), minor (in %) and trace elements (in ppm) of ceramic samples: data are normalized to 100% (LOI-free)*

	IB1	*IB2*	*IB3*	*IB4*	*IB5*	*IB6*	*IB7*	*IB8*	*IB9*	*IB10*	*IB11*	*IB12*	*IB13*	*IB14*	*IB15*	*IB16*	*IB17*	*IB18*	*IB19*
SiO_2	53.19	63.02	53.31	52.13	56.85	52.45	47.20	58.64	58.87	52.21	56.46	56.81	57.42	58.02	53.43	48.71	48.62	48.66	55.20
TiO_2	0.92	0.74	0.79	0.83	1.00	0.65	0.81	0.93	1.09	0.74	0.71	0.88	1.03	0.90	0.86	0.68	0.67	0.68	0.78
Al_2O_3	23.36	19.42	22.74	20.09	23.61	23.96	19.56	23.02	21.55	16.34	22.90	23.47	21.99	20.57	20.88	17.41	17.53	17.48	21.28
Fe_2O_3	7.92	5.68	9.07	7.06	6.06	7.01	7.03	5.93	6.88	6.79	7.19	6.14	9.15	7.68	6.90	5.27	5.21	5.33	6.60
MnO	0.07	0.04	0.03	0.09	0.04	0.05	0.09	0.03	0.05	0.13	0.04	0.04	0.13	0.05	0.08	0.03	0.04	0.03	0.04
MgO	2.57	1.70	4.59	3.60	2.88	3.34	3.28	3.14	2.62	3.42	2.92	2.89	2.43	3.48	3.01	2.78	2.89	2.78	3.37
CaO	5.45	4.42	3.35	11.43	3.35	5.51	16.18	1.71	3.29	15.31	3.02	2.97	1.89	3.22	8.71	19.15	18.74	19.03	7.23
Na_2O	0.59	0.58	0.97	0.69	1.07	1.12	0.86	1.06	0.73	1.16	0.97	1.03	0.89	0.89	0.93	0.61	0.94	0.82	0.74
K_2O	5.69	4.23	5.01	3.89	4.97	5.71	4.71	5.35	4.63	3.59	5.21	5.64	4.95	4.91	4.87	5.12	5.12	4.97	4.61
P_2O_5	0.22	0.17	0.14	0.19	0.16	0.18	0.28	0.17	0.30	0.32	0.58	0.12	0.13	0.28	0.32	0.23	0.23	0.22	0.16
	100	100	100	100	100	100	100	100	100	100	100	100	100	100	100	100	100	100	100
LOI	3.27	6.75		5.01		4.97	3.01			6.55	2.03	4.97				12.01	11.99	14.01	7.02
Ni	86	50	79	68	61	62	66	60	68	105	62	52	71	62	65	48	48	47	62
Cu	51	58	67	59	69	68	68	71	60	86	71	56	61	61	61	59	55	59	67
Zn	102	67	201	135	272	146	137	237	363	129	137	218	138	134	145	99	103	103	204
Rb	244	99	106	71	97	86	77	117	78	142	86	91	91	73	81	63	64	60	67
Sr	271	366	333	922	536	497	1319	454	362	617	625	407	314	263	528	725	609	558	441
Y	35	21	10	11	13	11	9	12	16	21	12	10	8	8	10	8	9	8	12
Zr	185	306	182	215	221	149	195	187	241	187	198	220	200	185	230	203	204	197	182
Nb	17	11	10	n.d.	11	n.d.	n.d.	10	11	14	n.d.	8	8	8	9	n.d.	n.d.	n.d.	n.d.
Ba	935	431	700	555	1326	742	638	627	878	802	812	609	871	591	1120	543	367	358	546

Table 2 *(Continued)*

	IB20	*IB21*	*IB22*	*IB23*	*IB24*	*IB25*	*IB26*	*IB27*	*IB28*	*IB29*	*IB30*	*IB31*	*IB32*	*IB33*	*IB34*	*IB35*
SiO_2	53.20	50.99	53.08	50.75	46.88	51.30	57.78	52.21	49.20	56.32	54.86	51.49	48.81	54.21	53.16	54.69
TiO_2	0.71	0.71	0.74	0.85	0.69	0.46	0.82	0.75	0.83	0.89	0.76	0.87	0.84	0.76	0.73	0.77
Al_2O_3	22.67	20.34	22.64	20.97	17.99	24.21	21.10	20.83	21.64	21.84	14.98	21.08	21.92	21.47	20.45	22.79
Fe_2O_3	7.52	6.94	7.06	7.24	7.65	8.37	6.77	7.18	7.66	7.70	6.47	7.35	7.43	6.81	7.57	7.38
MnO	0.04	0.06	0.04	0.12	0.07	0.04	0.05	0.05	0.10	0.04	0.05	0.12	0.11	0.06	0.04	0.07
MgO	4.42	5.81	3.40	3.14	3.46	1.85	4.13	5.30	3.08	3.98	2.73	3.57	2.96	3.57	4.69	1.66
CaO	5.69	8.98	6.30	10.74	17.06	6.60	3.22	7.43	10.37	3.63	14.35	8.71	11.01	6.65	6.80	7.13
Na_2O	1.05	0.88	0.93	0.92	0.63	1.11	0.94	0.89	0.88	1.02	0.49	1.30	1.06	0.86	0.88	1.19
K_2O	4.55	4.87	5.60	5.01	5.28	5.63	4.93	5.12	6.00	4.41	5.10	5.32	5.68	5.34	5.45	4.14
P_2O_5	0.16	0.42	0.21	0.26	0.28	0.42	0.27	0.24	0.24	0.18	0.21	0.20	0.17	0.28	0.23	0.19
	100	100	100	100	100	100	100	100	100	100	100	100	100	100	100	100
LOI		5.01	5.03	4.02			3.09			2.13	5.85	5.08	4.54	3.68	1.95	2.82
Ni	66	67	69	70	55	78	65	64	72	65	62	70	66	66	70	63
Cu	75	78	76	69	55	66	60	71	71	61	62	63	74	68	67	65
Zn	152	141	157	138	104	101	131	145	155	264	76	139	142	138	138	105
Rb	84	74	88	84	59	103	155	87	95	184	158	172	186	161	157	154
Sr	1169	777	643	590	870	816	333	542	766	393	463	402	569	409	304	312
Y	13	10	10	10	7	14	26	13	10	25	23	18	18	22	28	32
Zr	215	147	133	203	118	124	198	195	193	222	236	199	200	193	164	276
Nb	n.d.	n.d.	n.d.	n.d.	n.d.	n.d.	16	n.d.	n.d.	20	18	16	18	15	13	18
Ba	699	582	660	1111	665	872	670	725	848	587	1522	590	608	590	548	466

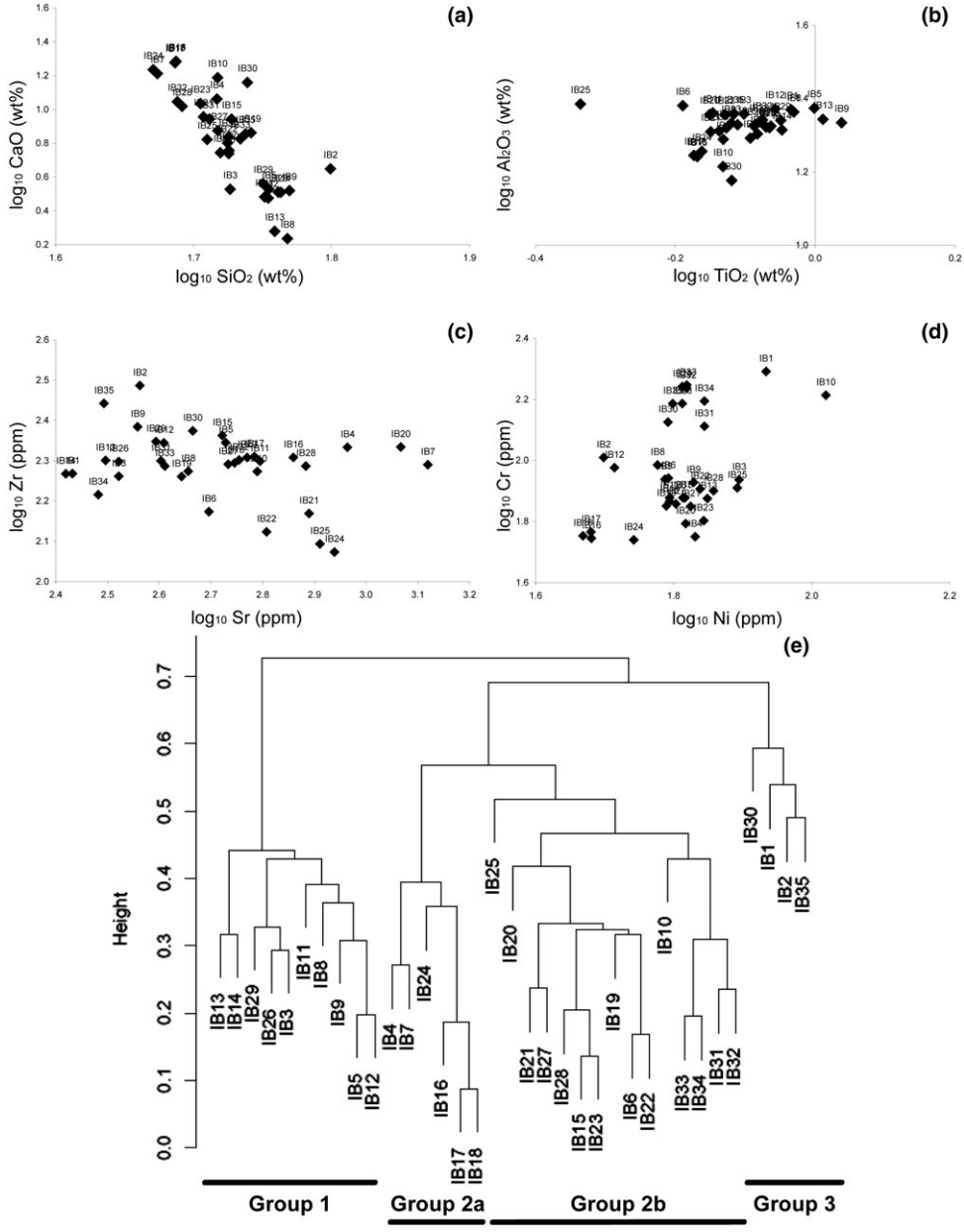

Figure 2 *Binary variation diagrams of log_{10}-transformed data of some major (a), minor (b) and trace element (c, d) concentrations; together with a dendrogram (e) showing the groups of samples obtained by statistical analyses.*

by considering the variables with the highest scores for each component, the data set was reduced and the calculation was simplified. We carried out a numerical analysis using the following selected variables: SiO_2, Fe_2O_3, CaO, MgO, Na_2O, K_2O, Cu, Zn, Rb, Sr and Zr.

The second step of the statistical calculation was the hierarchical cluster analysis (HCA), the results of which are set out in the dendrogram in Figure 2 (e) (*Euclidean* distance, *average*

Table 3 *Principal component analysis eigenvalues (C) of Cumulative Proportion*

	C. 1	*C. 2*	*C. 3*	*C. 4*	*C. 5*	*C. 6*	*C. 7*	*C. 8*	*C. 9*	*C. 10*	*C. 11*	*C. 12*	*C. 13*	*C. 14*
Cumulative Proportion	0.071	0.143	0.214	0.286	0.357	0.429	0.500	0.571	0.643	0.714	**0.786**	0.857	0.929	1.000

method). The dendrogram defines three different groups, one of which (Group 2) is divided into two subgroups. Group 1 includes a homogeneous series of 10 samples characterized by low calcium content: calcium oxide ranges from 1.7 wt% (IB8) to 3.6 wt% (IB29). Consequently, on average, they show high SiO_2 values (from 53.3 in IB3 to 58.9 in IB9). Group 1 is also often characterized by lower Sr content with respect to the other groups. The second group includes all the samples with moderate to high calcareous content. Group 2a is constituted by samples with a high CaO content (more than 10 wt%) and with the lowest SiO_2 values (IB4, IB7, IB16, IB17, IB18 and IB24). This group can also be distinguished because of its higher Sr content (with some scattered exceptions), compared to the other groups. Group 2b is the most numerous (15 samples) and includes samples with moderate calcium content (from 6.3 to 11 wt%), even if some of them (i.e., IB10, IB20 and IB25) have some peculiar compositional aspects. In fact, sample IB10 shows a CaO content typical of Group 2a (15.3 wt%), but the SiO_2 (52.2 wt%), Ni (105 ppm), Rb (142 ppm) values are higher and the Al_2O_3 (16.3 wt%) and Sr (617 ppm) contents are lower, compared with the samples in Group 2a. Sample IB25 is worthy of special mention, as it has the highest Al_2O_3 content (24.2 wt%) and one of the lowest MgO (1.8 wt%) and Zr (124 ppm) contents of all the samples. Sample IB20 is characterized by the highest Sr content (1169 ppm). This subgroup contains two of the three possible Phoenician amphorae (IB19 and IB34). The other sample, IB9, is quite different in chemical terms and falls into Group 1.

The last group of samples, Group 3, is the smallest and comprises the two small Visigoth wheels (IB1 and IB2) and two Iberian amphorae (IB30 and IB35). In particular, IB30 has a CaO content comparable with that of samples from Group 2a, although it has a higher silica content and a lower Sr content. Samples IB1 and IB2 are similar in composition and the differences lie in the SiO_2 (higher in IB2, 63 wt%) and Al_2O_3 (23.4 wt% in IB1, but 19.4 wt% in IB2) values. As regards trace elements, IB1 has a higher Rb (244 ppm) content. Finally, sample IB35 has a similar chemical composition to those in Group 2b, except that it has a lower Sr content (312 ppm) and higher Zr (276 ppm) values.

Table 4 shows the chemical characteristics of the samples in terms of the average (A) and the standard deviation (SD). The samples listed in this and subsequent tables are divided into the groups defined above.

Polarized optical microscopy and field emission scanning electron microscopy

The most striking textural characteristics of the ceramics that we studied using optical microscopy are summarized in Table 5. The main petrographic features of each group can be summarized as follows:

• *Group 1*. This group is rich in quartz and illite–muscovite phases, which are found as isolated crystals or as constituents of fragments of gneisses and mica-schists (Fig. 3 (a)). Sporadic plagioclases twinned according to the albite law are also visible. Isolated crystals of epidote,

Table 4 *Averages (A) and standard deviations (SD) within the defined group of samples after statistical treatment of XRF data*

	Group 1		*Group 2a*		*Group 2b*		*Group 3*	
	A	*SD*	*A*	*SD*	*A*	*SD*	*A*	*SD*
SiO_2	57.05	1.58	49.28	2.35	52.18	1.69	56.44	4.45
TiO_2	0.90	0.11	0.74	0.07	0.73	0.12	0.80	0.09
Al_2O_3	22.28	1.02	18.16	1.41	21.94	1.36	20.14	3.85
Fe_2O_3	7.26	1.16	6.51	1.00	7.25	0.50	6.86	0.99
MnO	0.05	0.03	0.07	0.04	0.06	0.03	0.06	0.01
MgO	3.31	0.71	3.24	0.33	3.67	1.17	2.17	0.56
CaO	2.96	0.64	16.29	2.78	7.76	1.87	7.84	4.48
Na_2O	0.96	0.10	0.85	0.19	0.95	0.12	0.71	0.32
K_2O	5.00	0.35	4.60	0.69	5.20	0.50	4.79	0.74
P_2O_5	0.23	0.14	0.26	0.05	0.26	0.10	0.20	0.02
Ni	64.46	7.05	64.74	21.58	67.43	5.04	65.25	15.04
Cu	63.75	5.48	63.72	11.92	70.12	5.24	59.00	6.06
Zn	209.64	77.18	118.51	16.92	148.42	25.29	87.50	18.88
Rb	107.74	35.59	78.91	31.69	84.95	10.18	163.75	59.89
Sr	402.08	109.82	815.75	288.60	676.95	215.23	353.00	83.01
Y	13.96	6.51	10.84	5.11	11.15	1.49	27.75	6.80
Zr	205.46	19.64	185.83	34.51	177.01	36.57	250.75	52.38
Nb	11.49	4.01	3.17	5.31	1.78	2.47	16.00	3.37
Ba	767.16	225.82	564.18	175.11	790.41	198.88	838.50	510.33

garnet, graphite and, above all, hornblende are also identified. It is interesting to notice that black cores were only observed in this group (Table 5).

• *Group 2a*. Quartz and muscovite crystals show the same morphologies and birefringences of the previous group. Sporadic epidote, hornblende and graphite phases were also identified. The main difference compared with Group 1 is the presence of carbonate grains. The most striking finding in these grains was the remains of bivalves, discovered in samples IB7 and IB16 (Fig. 3 (b)).

• *Group 2b*. A striking feature of this group is the absence of highly vitrified samples. The samples do not contain fragments of mica-schists either. Quartz is the most common mineral phase, followed by phyllosilicates and carbonates. Among accessory minerals, epidote seems to prevail over hornblende and some zircon crystals were also detected.

• *Group 3*. The two samples from Group 3 studied with this technique are the only ones with a coarse texture and have pores that vary from large to very large in size. The most common minerals are quartz and muscovite-like phases.

From a more general perspective, quartz is the main component of the temper of the ceramic pieces and has an angular shape of varying size, from just a few micrometres to 2–4 mm (in the case of the gneiss fragments). This mineral is a natural component of the sediments transported along the sub-basin of the River Baza from the erosion of Nevado-Filabrides and Alpujarrides metamorphic rocks, and it is commonly found in similar-sized grains in the clayey material of the area around Basti (Sebastián Pardo 1979; Vera *et al*. 2004). This indicates that quartz, gneiss and micashist fragments were not added by potters but were already present.

Muscovite-type phyllosilicates can often be observed aligned perpendicular to the direction of the pressure exerted on the clayey raw material during the moulding phase (Fig. 3 (c)). The

Table 5 *The main textural features of the ceramic samples. The samples of each group are ordered by vitrification degree. Q, G, M and C are, respectively quartz, gneiss, mica-schist and calcite temper fragments (in each sample, they are ordered by abundance from the higher to the lower); VL, L, S, VS, I, R and E refer, respectively, to very large, large, small, very small, irregular, rounded and elongated-shaped pores*

Group	*Sample*	*Temper*	*Matrix*	*Vitrification*	*Black core*	*Phyllosilicates birefringence*	*Pore shape*
1	IB5	Q, G	Fine	Low		Intermediate	S, E
	IB12	Q, G	Fine	Low		High	S, I
	IB14	G, Q, M	Fine	Low	Yes	High	L, I
	IB26	G, Q	Fine	Low	Yes	High	L, I
	IB8	Q, G	Fine	Intermediate	Yes	Intermediate	L, E
	IB9	Q, G, M	Fine	Intermediate	Yes	Intermediate	S, R
	IB13	Q	Fine	High		Low	S, E
	IB29	Q, G, M	Intermediate	High	Yes	Low	S, E
	IB3	Q	Very fine	Very high		Low	S, E
2a	IB4	Q, C	Fine	Low		High	S, I
	IB7	Q, G, M, C	Fine	Low		High	S, I
	IB16	Q, C	Very fine	Low		High	VS, R
	IB24	Q, G	Fine	High		Intermediate	S, R
2b	IB19	G, Q	Fine	Low		High	S, I
	IB20	Q	Fine	Low		High	S, R
	IB21	Q, G	Fine	Low		High	S, R
	IB28	Q, C	Very fine	Low		High	S, I
	IB33	Q, G	Very fine	Low		High	S, I
	IB15	Q, G, C	Intermediate	Intermediate		Intermediate	S, I
	IB23	G, Q, C	Fine	Intermediate		Intermediate	S, R
	IB31	G, G	Fine	Intermediate		High	S, E
	IB32	Q, G, C	Very fine	Intermediate		High	VS, E
3	IB2	G, Q, M	Coarse	Low		High	L, R
	IB1	M, G, Q	Coarse	High		Low	VL, I

birefringence of the phyllosilicates helped us to estimate the firing temperature of the samples studied, since birefringence falls as temperature increases (Cultrone *et al*. 2001). The least birefringent phyllosilicates were observed in samples IB1, IB3, IB13 and IB29, which suggests that these ceramics were fired at high temperatures. The presence of accessory minerals (hornblende and epidote, garnet, graphite, rutile and zircon; Fig. 3 (d)) confirms that the raw material comes from Nevado-Filabrides metamorphic rocks (Vera *et al*. 2004). Fe hydroxides and oxides and metal ores are frequently observed.

As with the quartz grains, the presence, size and morphology of the carbonate grains are compatible with the composition of the sediments from the River Baza around the archaeological area of Basti (Vera *et al*. 2004). The finding of carbonate grains in ceramic samples indicates low-to-moderate firing temperatures (Boynton 1980).

The pores vary considerably in terms of shape and size. In some cases it is interesting to note pores that are folded over, because the potter wanted to mould the piece into a certain shape (Fig. 3 (e)). We also observed darker halos around certain pores, which may indicate a higher heat flux, leading to localized enhanced vitrification. As for the degree of vitrification, the matrix of the samples is mainly red or yellow, and darker, almost black, colours are only detected in the highly vitrified samples IB1, IB3 and IB13. As regards the amphorae of possible Phoenician origin, the main difference was the presence of mica-schist fragments only in sample IB9.

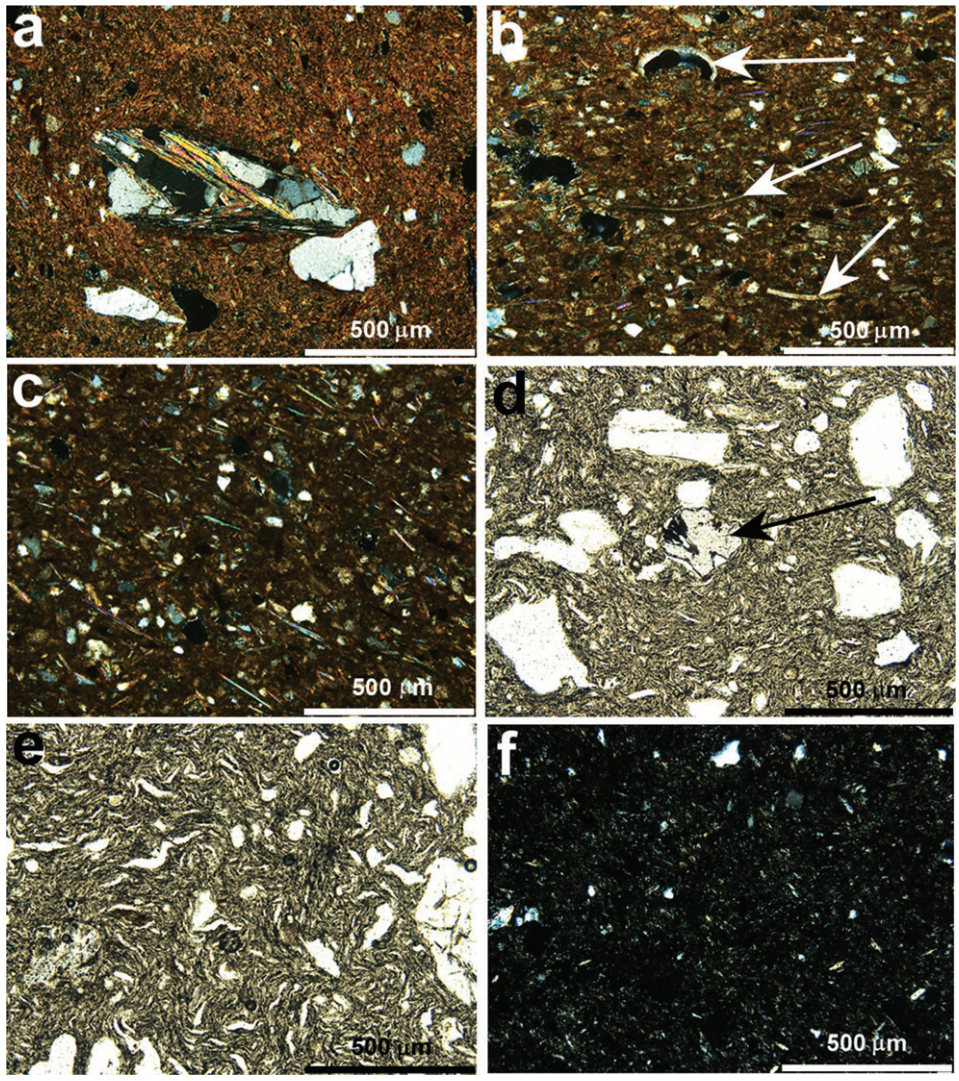

Figure 3 *Optical microscopy micrographs of: (a) a gneiss fragment with birefringent muscovite crystals; (b) the remains of bivalves (white arrows) in the matrix of sample IB16; (c) the orientation of small phyllosilicate laminae due to compression during moulding; (d) a garnet crystal (black arrow) in the matrix of sample IB8; (e) pores folded due to a moulding process in sample IB8; and (f) a high degree of vitrification in sample IB3.*

The mineralogy of two of the three Iberian plates found in different sites was similar to that of the pieces from Basti, the only difference being in the degree of firing, as one piece (IB3) was more vitrified than the other two (Fig. 3 (f)), and carbonate grains were only found in sample IB4. The FESEM observations allowed us to distinguish an initial porosity produced during the moulding of the pieces (Fig. 4 (a)), and a secondary porosity associated with the firing and sinterization process, and a leak of fluids (or gases) from the clayey minerals (Cairo *et al*. 2001) (Fig. 4 (b)). The images show that the phyllosilicates have a shape and composition typical of unaltered Al-rich mica in low-fired samples. The only thing visible at this scale

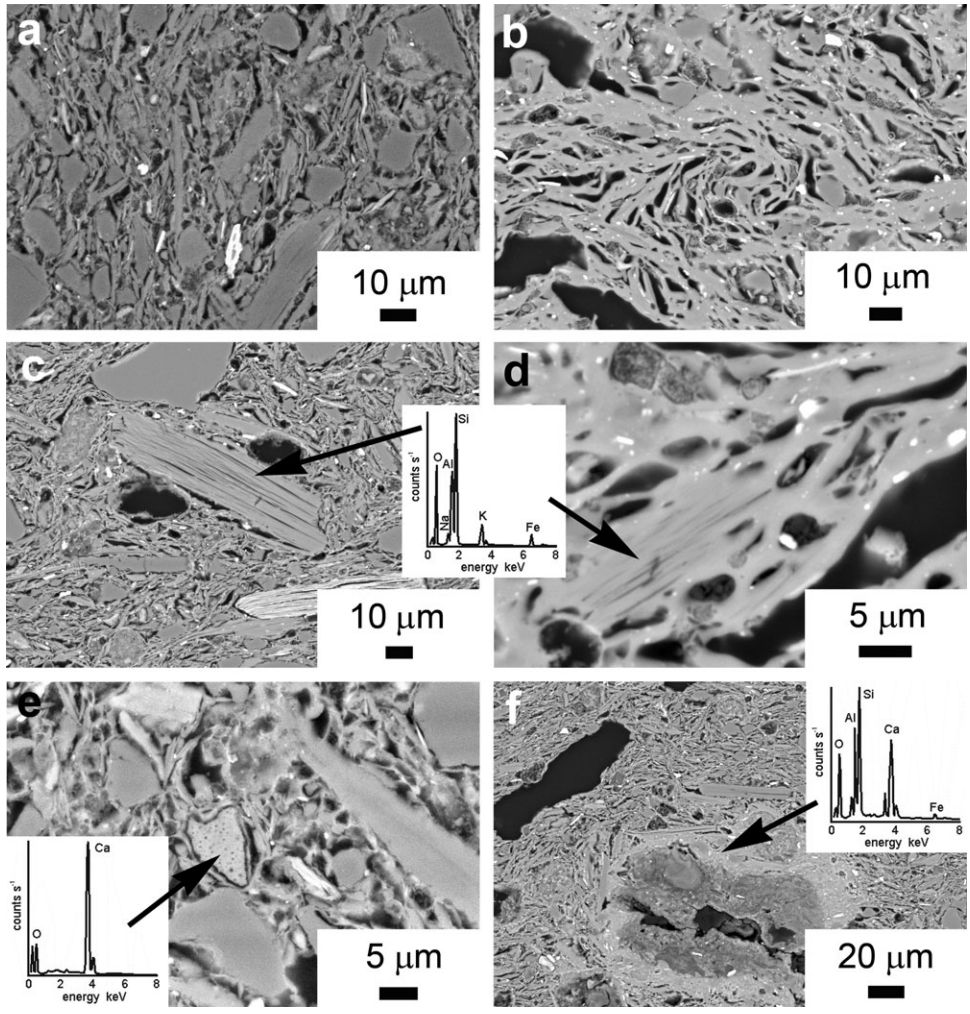

Figure 4 *Representative BSE images and EDS analyses of ceramic samples: a) a general view of a ceramic in which primary porosity and alienation of planar minerals are visible; (b) the development of secondary porosity due to a partial vitrification of the matrix; (c) the typical habit of phyllosilicates (see EDS analysis)—a separation along basal planes is visible; (d) a phyllosilicate crystal, showing clear evidence of melting progressing from the outside to the inside and indicated by the development of bubbles; (e) calcite crystals in low-fired ceramic samples; and (f) bright reaction rims around carbonate crystals in high-fired ceramics (see EDS analysis).*

is the separation of the laminae according to the planes (001) due to the dehydroxylation of the muscovite (Fig. 4 (c)). When samples are fired at higher temperatures, partial melting of phyllosilicates is visible (Fig. 4 (d)) and the formation of new silicate phases (i.e., mullite) can be presumed. Calcite grains are identified in CaO-rich samples (Fig. 4 (e)). As the firing temperature increases, the development of borders of reaction with the adjacent silicates can be noticed, which microanalyses have confirmed are due to the formation of calcium silicates (Fig. 4 (f)). Small bright hematite, rutile or zircon crystals were also identified in almost all the

samples. At a microtextural level, no significant differences were observed on the basis of the ages and types of the ceramics.

X-ray diffraction

Not all of the phases identified by polarized optical microscopy coincide with those detected using XRD, due to their low concentration and/or small size. XRD analysis was able to differentiate the 35 samples into Ca-poor and Ca-rich ceramics, depending on their mineralogical composition, and this is confirmed by the CaO content figures set out in Table 2. The Ca-poor ceramics were composed of quartz, variable amounts of phyllosilicates (illite/muscovite) and feldspars, low concentrations of hematite and, in seven samples, mullite; the Ca-rich ceramics contained quartz, illite, feldspar and hematite as in the previous group plus calcite, sporadic dolomite and, in eight cases, gehlenite and diopside (Table 6).

If this technique was not as decisive as XRF in differentiating ceramic clusters (no clear differences are discernible in relation to the mineralogy of the three previously defined groups), conversely it was crucial for estimating the temperatures at which the pieces were fired. The procedure followed for this estimate was based on the presence or absence of mineral phases such as illite, which suggests firing temperatures of lower than 900°C (Guggenheim *et al*. 1987; Cultrone *et al*. 2001); and calcite, which when it is not from a secondary source can indicate temperatures of up to 850°C, while dolomite decomposes earlier (700°C; Boynton 1980). As regards the development of new silicate phases, mullite indicates that ceramics were fired at temperatures over 900°C (Buys and Oakley 1993; Rodríguez Navarro *et al*. 2003), and in Ca-rich ceramics the presence of gehlenite and diopside suggests that temperatures of 900–1000°C were reached (Maniatis *et al*. 1981, 1983). When studying the firing temperatures, we also bore in mind the presence of amorphous or vitreous phases detected from the 'background noise' of the diffractograms. A louder noise could mean an increase in non-crystalline phases, something that occurs in ceramics when the firing temperature is increased (Huertas *et al*. 1991). The diffractograms with the loudest background noise were those for the samples IB1a, IB24, IB27, IB29 and, above all, IB3.

In sample IB1, we carried out a diffractometric analysis of the external (a) and internal (b) areas of the piece because, as indicated earlier, these surfaces had different colours—black and red, respectively. In mineralogical terms, the difference lies in the presence of mullite and in a higher background noise in the diffractogram (i.e., greater vitrification) for the external surface of the piece. Presumably, the outside of the piece was in contact with the fire for longer and was gradually burnt (Tite 1995; Wolf 2002).

Gypsum was only detected in one sample (IB7). This undoubtedly was of secondary origin and crystallized during the period in which the piece lay buried. Dolomite was detected in samples IB7 and IB21, which means—according to research by Boynton (1980)—that these two amphorae must have been fired at the lowest temperatures of the 35 samples. In IB10, calcite is of secondary origin because its presence is not compatible with peaks of gehlenite and diopside phases (Capel *et al*. 1985; Cultrone *et al*. 2001).

On the basis of XRD study supported by optical microscopy and FESEM observations, we have been able to establish the firing temperature of the 35 ceramic fragments (Table 7). If we consider the classification proposed by Tsantini *et al*. (2005), in which Iberian amphorae were divided into low-, well- and overfired depending on their estimated firing temperature, most of our pieces appear to have been well fired. In Table 7, we divided the pieces into four temperature groups, labelled from A (lowest fired) to D (highest fired). Only in two cases (IB7 and IB21) can the samples

Table 6 *XRD analysis of ceramic samples, ordered in each group by their identification label: Qtz, quartz; Phy, phyllosilicates (in general); Cal, calcite; Dol, dolomite; Hem, hematite; Fds, feldspars (in general); Geh, gehlenite; Di, diopside; Mul, mullite; Gyp, gypsum; m, melt; tr, traces; x, scarce; xx, abundant; xxx, very abundant (mineral symbols after Kretz 1983)*

Group	*Sample*	*Qtz*	*Phy*	*Cal*	*Dol*	*Hem*	*Fds*	*Geh*	*Di*	*Mul*	*Gyp*	*m*
1	IB3	xxx	tr				xx			x		x
	IB5	xxx	xx				x					
	IB8	xxx				tr	x			x		
	IB9	xxx	tr			tr	x			tr		
	IB11	xxx	x			tr	x			tr		
	IB12	xxx	xx			tr	x					
	IB13	xxx	tr			tr	x			x		
	IB14	xxx	x			x	x					
	IB26	xxx	x			tr	xx					
	IB29	xxx	tr			x	x			x		x
2a	IB4	xxx	x	xx			x					
	IB7	xxx	tr	x	x	x	x				xx	
	IB16	xxx	x	xxx			x					
	IB17	xxx	xx	xxx			x					
	IB18	xxx	x	xxx		tr	x					
	IB24	xxx	tr				x	xx	x			x
2b	IB6	xxx	xx				xx					
	IB10	xxx	tr	x			xx	x	x			
	IB15	xxx	tr			tr	x	tr	x			
	IB19	xxx	x				xx					
	IB20	xxx	tr			tr	xx					
	IB21	xxx	xx	x	tr	tr	x					
	IB22	xxx	xx				xx					
	IB23	xxx	tr			x	xx	x	tr			
	IB25	xxx	xx			tr	xx					
	IB27	xxx	tr				x	x	x			x
	IB28	xxx	xx	xx		x	x					
	IB31	xxx	x			tr	x	tr	tr			
	IB32	xxx	xx			x	x	tr	tr			
	IB33	xxx	xx				xx					
	IB34	xxx	x			tr	x					
3	IB1a	xxx				tr	x			tr		x
	IB1b	xxx				x	x					
	IB2	xxx	x			tr	xx					
	IB30	xxx					x	xx	x			
	IB35	xxx	x				x					

be classified as low-fired, and while initially no samples can be classified as overfired, in three samples (IB1, IB8 and IB30) in which phyllosilicates are totally decomposed, overfiring may have occurred. In spite of all this, it is important to remember that temperature variations of several hundred degrees are possible inside the oven during any one firing (Tite 1995).

Mercury intrusion porosimetry

This technique is not considered to be very useful for establishing the temperature at which a piece was fired or where its raw materials came from (Wolf 2002), but it does provide valuable

Table 7 *Estimated temperature (in °C) of ceramic samples after mineralogical and textural analyses. Temperature legend: A = 700–750°C; B = 751–850°C; C = 851–950°C; D > 950°C*

Group 1		*Group 2a*		*Group 2b*		*Group 3*	
Sample	*Temperature*	*Sample*	*Temperature*	*Sample*	*Temperature*	*Sample*	*Temperature*
IB5	B	IB7	A	IB21	A	IB2	B
IB12	B	IB4	B	IB6	B	IB35	B
IB14	B	IB16	B	IB19	B	IB1	D
IB26	B	IB17	B	IB20	B	IB30	D
IB9	C	IB18	B	IB22	B		
IB11	C	IB24	D	IB25	B		
IB3	D			IB28	B		
IB8	D			IB33	B		
IB13	D			IB34	B		
IB29	D			IB31	C		
				IB32	C		
				IB15	D		
				IB10	D		
				IB23	D		
				IB27	D		

information about the porosity and the distribution of the pore ranges, key parameters for predicting the technological characteristics of the ceramics (Cultrone *et al*. 2005; Grifa *et al*. 2005). Considering that porosity decreases with rising temperature as the spaces between clay particles shrink (and vitrification increases), especially when raw materials without carbonates are used (Buys and Oakley 1993; Cultrone *et al*. 2004), the results provided by this technique can corroborate mineralogical and textural studies. All the samples show practically unimodal distribution of pore sizes, with a maximum peak at either 0.4–0.5 μm or at around 0.06–0.1 μm (Fig. 5 (a)). In some cases, a second family of pores can be detected with a size of less than 0.01 μm, although they make up a very small percentage of the total (Fig. 5 (b)). The most frequent porosimetric curves fall between these two cases; that is, with a maximum peak and a widening of the curve towards smaller pores (Fig. 5 (c)). The position of the maximum peak and the presence or absence of this second family of pores affects the surface area values (A, Table 8): indeed, when the maximum peak moves towards lower pore radius values and pores with radii of less than 0.01 μm begin to appear or increase in number, the surface area increases (see the values of A and of pores with a radius of less than 0.1 μm in Table 8).

The typology of the ceramic generally has no effect on the pore-size distribution. Only the two handles of Iberian amphorae stand out for the largest amount of pores with a radius of more than 1 μm. As for the open porosity, which ranges from 21% to 38%, approximately, there is no clear correlation between this value and the estimated firing temperature of Ca-rich ceramics proposed in Table 7. Nevertheless, Ca-poor ceramic temperatures are better linked to the P value. This is because the phyllosilicates in the matrix of this second group of samples (Ca-poor ceramics) are not involved in the formation of new Ca and/or Mg silicates (i.e., gehlenite and diopside) and a significant amount of H_2O can be released due to dehydroxylation, favouring a gradual vitrification (and a reduction of porosity) of these samples (compare values of the estimated temperature in Table 7 with the porosity in Table 8) as the temperature rises (Brearley and Rubie 1990;

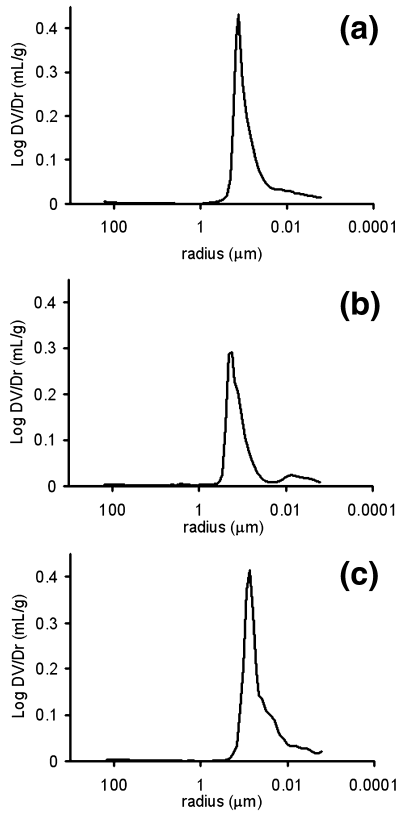

Figure 5 *MIP pore-size distribution curves (log differential intruded volume, in ml g^{-1}, versus pore radius, in μm) of (a) IB18, (b) IB4 and (c) IB6 ceramics.*

Cultrone *et al*. 2001). Generally, Ca-poor ceramics belonging to the temperature group B (Table 5) show a porosity of over 30% (only in one case, IB19, the porosity measured by MIP is ~28%); those in group C have porosity levels of between 23 and 30% (only in one case, IB11, the porosity was ~31%); and group D show a porosity of less than 23% (in two cases, IB3 and IB29, the porosity was ~28%).

Colorimetry

Figure 6 shows the chromatic values of the ceramic samples. They are represented using three different symbols, depending on their CaO content (Table 2). As can be seen, the highest a^* and b^* values (open squares) belong to ceramics without carbonates. The main factor influencing ceramic colour tends to be the formation of hematite. In the presence of carbonates, the iron is trapped in the structure of new calcium silicate phases, thus inhibiting the formation of hematite and producing yellowish colours (Klaarenbeek 1961; Maniatis *et al*. 1981; Kreimeyer 1987). Samples represented as open triangles (middle CaO content) and as open circles (high CaO content), tend to reduce b^* and, above all, a^* values. Five samples diverge from the general trend of ceramic colour and are characterized by low a^* and b^* values. Three of them create a small

Table 8 *MIP data of ceramic samples, divided into those with (YES) and without carbonates (NO) on the basis of XRF and XRD analyses and ordered in each group by their porosity values. A = surface area ($m^2\ g^{-1}$); ρ_a = apparent density ($g\ m^{-3}$); ρ_r = real density ($g\ m^{-3}$); P = porosity (%); >1 = pores with radius larger than 1 μm; 0.1–1.0 = pores with radii between 0.1 and 1 μm; <0.1 = pores with radii less than 0.1 μm*

Group	*Sample*	*Carbonates*	*A*	ρ_a	ρ_r	*P*	*>1*	*0.1–1.0*	*<0.1*
1	IB8	NO	10.81	2.01	2.60	22.64	14.2	55.7	30.1
	IB13	NO	13.76	2.05	2.65	22.75	3.7	35.5	60.8
	IB29	NO	6.55	1.89	2.62	27.96	6.3	72.6	21.1
	IB9	NO	10.98	1.89	2.65	28.50	4.4	71.4	24.2
	IB3	NO	7.79	1.85	2.59	28.58	3.8	70.3	25.9
	IB12	NO	15.61	2.01	2.90	30.67	7.1	7.7	85.2
	IB11	NO	8.39	1.72	2.50	31.21	3.7	73.6	22.5
	IB5	NO	7.53	1.37	2.01	32.11	5.6	77.8	16.6
	IB14	NO	10.94	1.24	1.88	33.69	9.3	70.4	20.3
2a	IB4	YES	10.98	1.87	2.62	28.56	3.6	66.0	30.4
	IB17	YES	7.81	1.72	2.51	31.55	3.2	61.9	34.9
	IB7	YES	10.96	1.79	2.68	33.06	1.5	82.1	16.4
	IB18	YES	15.17	1.71	2.57	33.70	2.0	52.4	45.6
	IB16	YES	14.29	1.63	2.47	33.98	2.6	57.7	39.7
2b	IB21	YES	15.45	1.81	2.42	24.95	2.8	50.5	46.7
	IB19	NO	24.43	1.85	2.57	27.95	4.8	11.0	84.2
	IB15	YES	11.24	1.76	2.56	31.46	2.8	61.9	35.3
	IB34	NO	10.44	1.77	2.66	33.21	4.3	67.7	28.0
	IB31	YES	12.06	1.76	2.66	33.65	2.5	74.0	23.5
	IB22	NO	22.33	1.66	2.54	34.93	2.1	13.6	84.3
	IB10	YES	7.58	1.67	2.58	35.39	4.7	75.7	19.6
	IB6	NO	20.73	1.68	2.61	35.69	2.2	13.8	84.0
	IB23	YES	13.84	1.74	2.74	36.53	2.1	77.0	20.9
	IB28	YES	17.89	1.74	2.76	37.14	2.0	32.1	65.9
	IB20	NO	8.53	1.67	2.68	37.71	1.5	83.8	14.7
	IB25	NO	14.37	1.59	2.55	37.72	2.0	79.7	18.3
	IB33	NO	15.42	1.62	2.60	37.80	1.9	65.3	32.8
	IB32	YES	12.07	1.69	2.74	38.32	3.2	72.2	24.6
	IB27	YES	17.81	1.61	2.62	38.45	1.6	70.1	28.3
3	IB30	YES	39.32	1.77	2.52	29.73	3.6	18.0	78.4
	IB35	NO	9.93	1.74	2.65	34.40	2.1	81.7	16.2

group highlighted by a dotted curve; they are the grey Iberian dish IB3, IB4 and IB5; the other two ceramics surrounded by another dotted curve, IB1 and IB2, are the Visigoth wheels. In both cases we are speaking of ceramics of the same age, with the same use and, as this technique confirms, of the same colour. It is also noticeable that the highest b^* contents belong to the handles of two Iberian amphorae (IB8 and IB14), which are of a similar age. As regards the samples of possible Phoenician origin, only two of them, IB19 and IB34, are close to each other. The IB9 sample is somewhat distant from the other two, which corroborates the results of statistical analyses (Fig. 2 (e)).

CONCLUSIONS

The study of the ceramics from the archaeological site of Basti (Granada, Spain) suggests that the clayey raw material used in the manufacture of the ceramic pieces was of local origin, and came

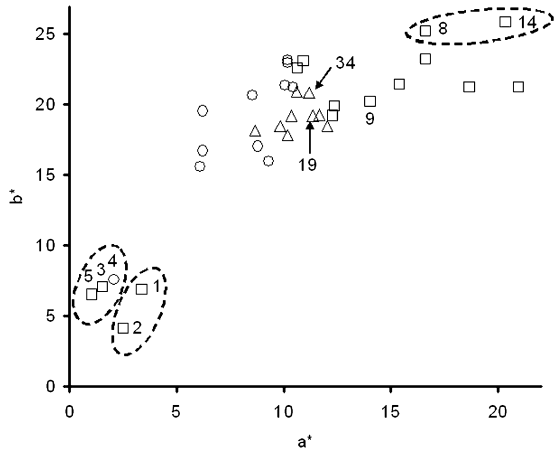

Figure 6 *The chromatic coordinates (a* and b*) of ceramic fragments. Open squares represent colour samples with CaO < 6 wt%; open triangles represent colour samples with 6 < CaO < 10 wt%; open circles represent colour samples with CaO > 10 wt%.*

from sediments from the River Baza. This is the first evidence for the knowledge that the Iberians possessed of the resources in the area around Basti. The ability to locate and use these resources was of great importance in a society where all commercial and administrative activities were controlled by each *oppidum*, which operated as a microstate within its area of influence (Adroher Auroux 2008).

The statistical treatment of chemical analyses enabled us to divide the samples into three main groups: Group 1, with 10 samples; Groups 2a and 2b, with 21 samples; and Group 3, the smallest of the three, with four samples. The petrographic study showed that the mineralogy and the texture of the samples were very similar and there were few differences between them (i.e., the absence of carbonates in Group 1 and the prevalence of hornblende and epidote fragments in Groups 1 and 2a). Our data suggest that the raw materials used came from the same area around Basti, because the mineralogy of the ceramics is closely compatible with that of the sediments in the Baza sub-basin. It seems that these early potters quarried the raw materials in two main areas, one of which was poor and the other moderate-to-rich in carbonates, depending on the specific purpose of the ceramic that they were making or the appearance they wanted to achieve, but in some cases another supply area, close to the main areas—but possibly smaller or more difficult to reach—was also used. These three areas had to be active contemporaneously, because the range of ages of all the ceramics is very similar.

Colorimetric analysis revealed that the use of a raw material poor, moderate or rich in carbonates influenced the visual aspect of the fired pieces, turning them from red to yellow. This technique allowed us to group ceramics with the same use within specific areas on the diagram, thereby confirming their similarities. We estimated the firing temperatures on the basis of the mineralogy and the degree of vitrification of ceramics. These were generally between 750 and 950°C, which means that they were well fired. Only two samples were low fired and, perhaps, three others were overfired. The presence of new silicate phases (mullite, gehlenite and diopside) was observed several times.

In view of the fact that ceramic was one of the distinctive aspects of Iberian culture, we believe that our research contributes to a greater understanding of how these people lived. The obtaining

of well-fired samples suggests that the local population had a broad knowledge of the use of natural resources as well of the construction and use of kilns. Moreover, the absence of 'lime blowing' in well-fired ceramics rich in carbonates suggests a degree of ingenuity on the part of the potters, who had devised a means of preventing their products from breaking (e.g., by grinding the carbonate fragments before firing, or cooling recently fired ceramics in water; Cultrone *et al*. 2004). 'Black cores' had developed in several samples of Group 1, which suggests a rapid firing of these pieces.

The samples studied presented two main populations of pores with a radius measuring 5 or 1 μm, approximately. Generally, neither the pore-size distribution nor the porosity was affected by the typology of the ceramics. However, the porosity and the firing temperature of Ca-poor ceramics are inversely correlated: as the temperature increases, the porosity decreases because of a gradual vitrification. The same correspondence was not found in Ca-rich ceramics. Primary porosity, fruit of the kneading of the raw material and the moulding of the pieces, was distinguished from secondary porosity, which developed during the vitrification of the matrix of certain pieces.

The fact that the potters had already achieved a high level of technological development may explain why no differences were found in ceramic production over the broad time interval studied (nine centuries). The two dishes, which had been found in two different archaeological sites near Basti, seem to be of local origin. The same conclusion can be reached for two of the three amphorae that were thought to be of Phoenician origin. This research confirms that with the combined use of geochemical, petrographic and physical techniques in the characterization of archaeological ceramic samples, it is possible to define a first reference group (as defined in Maggetti 2001) of Basti ceramics, thereby providing valuable information about their composition, technology and provenance.

ACKNOWLEDGEMENTS

This study was financially supported by Research Group RNM179 of the Junta de Andalucía and by Research Project MAT2008-06799-C03-03. We are grateful for the in-depth review by two anonymous referees and to Nigel Walkington for his assistance in translating the original text.

REFERENCES

Adroher Auroux, A. M., 2008, Un recorrido por la investigación del mundo ibérico en el Altiplano, in *Bastetania Ibérica: viaje arqueológico por las altiplanicies granadinas*, 13–20, Ayuntamiento de Baza and Asociación de Estudios de Arqueología Bastetana Eds., Baza.

Aruga, R., 2003, The problem of multivariate classification of samples with radial (or V-shaped) chemical data, *Talanta*, **60**, 37–44.

Baxter, M. J., 2001, Statistical modelling of artefact compositional data, *Archaeometry*, **43**, 131–47.

Boynton, R. S., 1980, *Chemistry and technology of lime and limestone*, 2nd edn, John Wiley & Sons, Inc., New York.

Brearley, A. J., and Rubie, D. C., 1990, Effects of H_2O on the disequilibrium breakdown of muscovite + quartz, *Journal of Petrology*, **31**, 925–56.

Buxeda i Garrigós, J., Jones, R. E., Kilikoglou, V., Levi, S. T., Maniatis, Y., Mitchell, J., Vagnetti, L., Wardle, K. A., and Andreou, S., 2003, Technology transfer at the periphery of the Mycenaean world: the cases of Mycenaean pottery found in the Central Macedonia (Greece) and the plain of Sybaris (Italy), *Archaeometry*, **45**, 263–84.

Buys, S., and Oakley, V., 1993, *Conservation and restoration of ceramics*, Butterworth-Heinemann, Oxford.

Cairo, A., Messiga, B., and Riccardi, M. P., 2001, Technological features of the 'Cotto Variegato': a petrological approach, *Journal of Cultural Heritage*, **2**, 133–42.

Capel, J., Huertas, F., and Linares, J., 1985, High temperature reactions and use of Bronze Age pottery from La Mancha, Central Spain, *Mineralogica Petrographica Acta*, **29A**, 563–75.

Cardell, C., Rodríguez Gordillo, J., Morotti, M., and Párraga, M., 1999, Arqueometría de cerámicas fenicias de 'Cerro del Villar' (Guadalhorce, Málaga): composición y procedencia, in *Arqueometría y Arqueología*, (ed. J. Capel Martínez), 107–20, Monográfica Arte y Arqueología, Universidad de Granada, Granada.

Cerdeño del Castillo, J., Díaz Rubio, R., Obis Sánchez, J., Pérez Lorenzo, A., and Velasco Vélez, J., 2000, *Manual de patologías de las piezas cerámicas para la construcción*, AITEMIN, Toledo.

Chen, G., and Wang, J., 1998, The preparation of marine geological certified reference materials—polymetallic nodule GSPN-1 and marine sediment GSMS-1 from the Central Pacific Ocean, *Geostandards and Geoanalytical Research*, **22**, 119–25.

Cultrone, G., Sidraba, I., and Sebastián, E., 2005, Mineralogical and physical characterization of the brick used in the construction of the 'Triangul Bastion', Riga (Latvia), *Applied Clay Science*, **28**, 297–308.

Cultrone, G., Rodríguez Navarro, C., Sebastián, E., Cazalla, O., and de la Torre, M. J., 2001, Carbonate and silicate phase reactions during ceramic firing, *European Journal of Mineralogy*, **13**, 621–34.

Cultrone, G., Sebastián, E., Elert, K., de la Torre, M. J., Cazalla, O., and Rodríguez Navarro, C., 2004, Influence of mineralogy and firing temperature on porosity of bricks, *Journal of the European Ceramic Society*, **24**, 547–64.

Di Martino, P., Farnetano, D., Grifa, C., Barattolo, F., Langella, A., Morra, V., Trojsi, G., and Tusa, S., 2005, Indagini mineralogiche e petrografiche su ceramiche neolitiche da Partanna (TP), in *Atti del Congresso AIAR 2006*, 131–44, Caserta.

Fabbri, B., and Gualtieri, S., 2007, Coarse ceramics with calcite inclusions: a technology for all ages, in *9th European Meeting on Ancient Ceramics*, Budapest.

Fabbri, B., Guarini, G., Arduino, E., and Coghe, M., 1994, Significato del fosforo nei reperti ceramici di scavo, in *Proceedings of the 1st European Workshop on Archaeological Ceramics*, 183–92.

Fernandes, F., Jordán, M. M., Martín, J. D., Sanfeliu, T., and Clausell, G., 1998, Estudio arqueométrico de cerámicas ibéricas del yacimiento del Torrelló de Almassora (Castellón), *Caesaraugusta*, **73**, 99–107.

Fernández, J., Viseras, C., and Soria, J., 1996, Pliocene–Pleistocene continental infilling of the Granada and Guadix basins (Betic Cordillera, Spain), in *Tertiary basins of Spain: the stratigraphic record of crustal kinematics* (eds P. F. Friend and C. Dabrio), 366–71, Cambridge University Press, Cambridge.

García Heras, M., Reyes Trujeque, J., Ruiz Guzman, R., Avilés Escaño, M. A., Ruiz Conde, A., and Sánchez Soto, P. J., 2006, Estudio arqueométrico de figurillas cerámicas mayas de Calakmul (Campeche, México), *Boletín de la Sociedad Española de Cerámica y Vidrio*, **45**, 245–54.

Gibert, L., Ortí, F., and Rosell, L., 2007, Plio-Pleistocene lacustrine evaporites of the Baza Basin (Betic Chain, SE Spain), *Sedimentary Geology*, **200**, 89–116.

Gil Julià, S., 2008, Lo sagrado de los bastetanos: entre la vida y la muerte, in *Bastetania Ibérica: viaje arqueológico por las altiplanicies granadinas*, 61–75, Ayuntamiento de Baza and Asociación de Estudios de Arqueología Bastetana Eds., Baza.

González Vílchez, M. C., González García, F., and García Ramos, G., 1985, Materias primas y datos tecnológicos de piezas cerámicas antiguas del yacimiento arqueológico de Cerro Macareno (Sevilla), *Boletín de la Sociedad Española de Cerámica y Vidrio*, **24**, 173–86.

Grifa, C., Langella, A., Morra, V., and Soricelli, G., 2005, 'Pantellerian Ware' from Miseno (Campi Flegrei, Naples), *Periodico di Mineralogia*, **74**, 69–86.

Grifa, C., Morra, V., Langella, A., and Munzi, P., 2009, Byzantine ceramic production from Cuma (Campi Flegrei, Napoli), *Archaeometry*, **51**, 75–94.

Guggenheim, S., Chang, Y. H., and Koster Van Groos, A. F., 1987, Muscovite dehydroxylation: high temperature studies, *American Mineralogist*, **72**, 537–50.

Hall, M. E., 2004, Pottery production during the Late Jomon period: insights from the chemical analyses of Kasori B pottery, *Journal of Archaeological Science*, **31**, 1439–50.

Hein, A., Day, P. M., Cau Ontiveros, M. A., and Kilikoglou, V., 2004, Red clays from central and eastern Crete: geochemical and mineralogical properties in view of provenance studies on ancient ceramics, *Applied Clay Science*, **24**, 245–55.

Huertas, J., Huertas, F., and Linares, J., 1991, Evolución de las fases no cristalinas en cerámicas arqueológicas por DRX, *Boletín de la Sociedad Española de Mineralogía*, **14**, 71–8.

Igea Romera, J., Lapuente Mercadal, P., Saiz Carrasco, M. E., Burillo Mozota, F., Pérez Arantegui, J., and Fanlo Loras, J., 2008, Methodology approach applied to characterize celtiberian pottery productions from central Iberian chain (Spain), in *37th International Symposium on Archaeometry* (eds I. Memmi Turbanti and R. Francovich), 149–50, Siena.

Klaarenbeek, F. W., 1961, The development of yellow colours in calcareous bricks, *Transactions of the British Ceramic Society*, **60**, 738–72.

Kreimeyer, R., 1987, Some notes on the firing colour of clay bricks, *Applied Clay Science*, **2**, 175–83.

Kretz, R., 1983, Symbols for rock-forming minerals, *American Mineralogist*, **68**, 277–9.

Maggetti, M., 2001, Chemical analyses of ancient ceramics: what for? *Chimia*, **55**, 923–30.

Maggetti, M., Galetti, G., and Schnalleuwly, R., 1988, Die Feinkeramik von Sissach-Brühl: eine spätlateinezeitliche Referenzgruppe, *Berichte aus der Arbeit des Amtes für Museen und Archäologie des Kantons Baselland*, **13**, 1–47.

Maniatis, Y., Simopoulos, A., and Kostikas, A., 1981, Mössbauer study of the effect of calcium content on iron oxide transformations in fired clays, *Journal of the American Ceramic Society*, **64**, 263–9.

Maniatis, Y., Simopoulos, A., Kostikas, A., and Perdikatsis, V., 1983, Effect of reducing atmosphere on minerals and iron oxides developed in fired clays: the role of Ca, *Journal of the American Ceramic Society*, **66**, 773–81.

Maritan, L., 2004, Archaeometric study of Etruscan–Padan type pottery from the Veneto region: petrographic, mineralogical and geochemical–physical characterisation, *European Journal of Mineralogy*, **16**, 297–307.

Martín, J. D., 2004, *XPowder, a software package for powder X-ray diffraction analysis*, Lgl. Dep. GR 1001/04.

Mirti, P., and Davit, P., 2004, New developments in the study of ancient pottery by colour measurement, *Journal of Archaeological Science*, **31**, 741–51.

Molera, J., Pradell, T., and Vendrell Saz, M., 1998, The colours of Ca-rich ceramic pastes: origin and characterization, *Applied Clay Science*, **13**, 187–202.

Nava, A., and Riccardi, M. P., 1999, Il colore come parametro termo-archeometrico nello studio dei manufatti ceramici antichi: alcuni dati sperimentali, in *6ª Giornata Le Scienze della Terra e l'Archeometria* (eds C. D'Amico and C. Tampellini), 21–6, Este.

Niembro Bueno, M. C., 2009, *Wavelength dispersive X-ray fluorescence analysis of major and trace elements in marine sediments by the fundamental parameters method: using geochemical proxies for paleoenvironmental reconstruction*, unpublished master's thesis, University of Granada.

Ordiozola, C. P., and Hurtado Pérez, V. M., 2007, The manufacturing process of 3rd millennium BC bone based incrusted pottery decoration from the Middle Guadiana river basin (Badajoz, Spain), *Journal of Archaeological Science*, **34**, 1794–803.

Pavía, S., 2006, The determination of brick provenance and technology using analytical techniques from the physical sciences, *Archaeometry*, **48**, 201–18.

Pérez-Peña, J. V., Azañón, J. M., Azor, A., Tuccimei, P., Della Seta, M., and Soligo, M., 2009, Quaternary landscape evolution and erosion rates for an intramontane Neogene basin (Guadix–Baza basin, SE Spain), *Geomorphology*, **106**, 206–18.

Petit Domínguez, M. D., García Giménez, R., and Rucandio, M. I., 2003, Chemical characterization of Iberian amphorae and tannin determination as indicative of amphora contents, *Microchimica Acta*, **141**, 63–8.

R Development Team, R. Version 1.1.0 for Mac, 2005, Freely available from http://microarrays.unife.it/CRAN/

Ricciardi, P., Nodari, L., Gualtieri, S., De Simone, D., Fabbri, B., and Russo, U., 2008, Firing techniques of black slipped pottery from Nepal (12th–3rd century B.C.): the role of Mössbauer spectroscopy, *Journal of Cultural Heritage*, **9**, 261–8.

Rodríguez Navarro, C., Cultrone, G., Sánchez Navas, A., and Sebastián, E., 2003, TEM study of mullite growth after muscovite breakdown, *American Mineralogist*, **88**, 713–24.

Sebastián Pardo, E. M., 1979, *Mineralogía de los materiales Plioceno-Pleistocenos de la depresión de Guadix–Baza (Granada)*, Ph.D. thesis, Secretaría de Publicaciones de la Universidad de Granada, Granada.

Scott, V. D., and Love, G., 1983, *Quantitative electron-probe microanalysis*, John Wiley & Sons, Inc., New York.

Soria, J. M., and Viseras, C., 2008, La Cuenca de Guadix. Rasgos geológicos generales. Vertebrados del Plioceno superior terminal en el suroeste de Europa: Fonelas P-1 y el Proyecto Fonelas (ed. A. Arribas), *Cuadernos del Museo Geominero*, **10**, 3–19.

Stepkowska, E. T., and Jefferis, S. A., 1992, Influence of microstructure on firing colour of clays, *Applied Clay Science*, **6**, 319–42.

Tite, M. S., 1995, Firing temperature. How and why? *KVHAA Konferenser*, Stockholm, **34**, 37–42.

Tsantini, E., 2007, *Estudi de la producció i la distribució d'àmfores ibèriques en el NE peninsular a través de la seva caracterització arqueomètrica*, unpublished Ph.D. thesis, Universitat de Barcelona.

Tsantini, E., Buxeda I Garrigós, J., Madrid Fernández, M., Gurt I Esparraguera, J. M., and Miñarro I Casas, M., 2005, Amphora production in the pre-Roman northeast of the Iberian peninsula and evidence of trade with the Balearic islands, in *Understanding people through their pottery* (eds M. I. Prudêncio, M. I. Dias and J. C. Waerenborgh), 279–86, Trabalhos de Arqueologia, 42, Insituto Português de Arqueologia, Lisbon.

Veniale, F., 1990, Modern techniques of analysis applied to ancient ceramics, in *Advanced workshop 'Analytical methodologies for the investigation of damaged stones'*, 1–45, Pavia.

Vera, J. A., Ancochea, E., Barnolas, A., Bea, F., Calvo, J. P., Civis, J., De Vicente, G., Fernández Gianotti, J., García Cortés, A., Pérez Estaún, A., Pujalte, V., Rodríguez Fernández, L. R., Sopeña, A., and Tejero, R., 2004, Introducción, in *Geología de España* (ed. J. A. Vera), 3–17, SGE–IGME, Madrid.

Viseras, C., Soria, J. M., and Fernández, J., 2004, Cuencas neógenas postorogénicas de la Cordillera Bética, in *Geología de España* (ed. J. A. Vera), 576–81, SGE–IGME, Madrid.

Wolf, S., 2002, Estimation of the production parameters of very large medieval bricks from St Urban, Switzerland, *Archaeometry*, **44**, 37–65.